Journal of
*Marine Science and Engineering*

MDPI

*Article*

# Concept Design of a 15 MW TLP-Type Floating Wind Platform for Korean Offshore Installation

**Sung Youn Boo [1], Yoon-Jin Ha [2], Steffen Allan Shelley [1], Ji-Yong Park [2], Chang-Hyuck Lim [2] and Kyong-Hwan Kim [2,*]**

[1] VL Offshore LLC, Houston, TX 77084, USA; sboo@vloffshore.com (S.Y.B.); sshelley@vloffshore.com (S.A.S.)
[2] Korea Research Institute of Ships & Ocean Engineering (KRISO), Daejeon 34103, Republic of Korea; yj_ha0811@kriso.re.kr (Y.-J.H.); jypark@kriso.re.kr (J.-Y.P.); ckdgur1092@kriso.re.kr (C.-H.L.)
* Correspondence: kkim@kriso.re.kr; Tel.: +82-042-866-3941

**Abstract:** Offshore wind farms on the east offshore of Korea to produce multi-GW power from floating wind platforms are being planned. The objectives of the present study are to develop a new TLP-type floating wind platform with a 15 MW turbine for the planned site and to confirm the feasibility of the TLP design under extreme typhoon environments. The concept design of the 15 MW TLP floating platform was completed for installation at a water depth of 137 m. The platform was vertically moored with highly pretensioned wire rope tendons. The platform and tendons were designed to withstand extreme conditions for up to 50 years. Additionally, a platform with an integrated turbine was designed to be wet-towable from the quayside without dedicated vessels to minimize the pre-service cost and risk. An extreme response analysis was conducted to evaluate the platform motion, acceleration, airgap and tendon tension for wave variation, intact and damaged condition of the tendon, environment heading change, and water level variation. The platform design results were validated using the design criteria from the industry standards and recommendations, and the design was verified to comply with the design requirements for the planned sites.

**Keywords:** TLP; floating offshore wind turbine; FOWT; tendon; extreme response analysis; concept design; global performance; design criteria



**Citation:** Boo, S.Y.; Ha, Y.-J.; Shelley, S.A.; Park, J.-Y.; Lim, C.-H.; Kim, K.-H. Concept Design of a 15 MW TLP-Type Floating Wind Platform for Korean Offshore Installation. *J. Mar. Sci. Eng.* **2024**, *12*, 796. https://doi.org/10.3390/jmse12050796

Academic Editors: Spyros A. Mavrakos and Dimitrios N. Konispoliatis

Received: 12 March 2024
Revised: 7 May 2024
Accepted: 8 May 2024
Published: 10 May 2024



## 1. Introduction

Floating offshore wind farms in the East offshore of South Korea near the Dong-Hae gas field are planned for targeting of 6 GW to 9 GW, with a large capacity of turbine (e.g., 15 MW).The current lease areas of the planned sites are in the pathway of frequent and strong tropical typhoons, and thus the wind farms require a robust platform design to survive in such an environment, in terms of their motions, structures, and mooring systems.

There are several platform candidates for the planned sites, such as semi-submersible (semi), TLP, spar, and other types of platforms (e.g., barge). A Semi platform might be a good candidate due to its technological maturity. A semi platform with a 15 MW turbine has recently been developed [1], and its operational performances were compared with the 15 MW reference semi platform [2]. The spar platform has some advantages over others once installed on site but requires a very deep sheltered area to integrate the turbine to the floating hull foundation and a deep operational water depth. Therefore, a spar with a large turbine may not be a feasible option for Korean offshore. As opposed to the semi or spar, a TLP-type wind platform is very stable in the motions of heave, roll, and pitch due to the action of the highly tensioned mooring system. Additional benefits of the TLP platform include a small mooring footprint and lighter weight compared to other types of platforms [3].

There are various designs of TLP foundations depending on the number of columns. Mono-column TLP has a long-submerged column for buoyancy and long spokes (or pontoons) to improve rotational stiffness with the tendons, including Blue H TLP [4],

OCEAN BREEZE TLP [5], MIT TLP [6], PELASTAR TLP [7], concrete ECO TLP [8], and Float4WindTM TLP with tubular pontoon members [9]. A different concept of mono-column TLP with a pendulum is also proposed [10]. The mono-column TLP has a relatively lightweight platform but inherent instability until the tendons are connected to the foundation. Therefore, it requires additional vessels or equipment to hold it upright for turbine integration, as well as tow and platform installation. To overcome those challenges, multi-column TLP wind platforms have been designed: four-column TLP [11], three column-TLP [12], ultra-deep-water TLP application [13], GICON-TLP fabricated with steel and concrete combination [14], concrete barge-type TLP [15], Tetra TLP with tubular structures [16], and Mars-Wind TLP with modular hull components [17,18].

A TLP mooring tendon can be fabricated with steel tubulars, steel wire ropes, or synthetic ropes. The wires and synthetic ropes are a more viable option over the steel pipe in terms of cost and installation, although steel pipe tendons have been used for all the offshore TLPs installed to date. The wire rope tendon offers benefits with more stable motions and lowering tensions than the synthetic alterative [19]. The wire tendon was also successfully implemented in the TLP platform [13,17].

For TLPs, wet-towability with self-stability is an import design factor for reducing transportation costs and risks, requiring the assurance of the TLP's resilience during the pre-service operations, from turbine integration to tendon connection on site. Additionally, designs should be tailored to suit severe typhoon environments on site, with lightweight tendons and platforms. With the consideration of those factors, for the present study, a 15 MW multi-column TLP-type wind turbine platform (KRISO-TLP) moored with the wire rope tendons was designed for the east offshore of Korea. Design features of the KRISO-TLP are as follows: (1) a shallow lightship draft with the turbine allows tow-out operations from shipyards in Korea, (2) the platform has a self-stability for wet-tow and installation, and (3) square-shape columns can facilitate hull fabrication at small shipyards. This approach may involve some hull weight penalties compared to the mono-column TLP but can remove all the costs, risks, and complex operations associated with pre-service execution.

The objective of the present study is the concept design of the KRISO-TLP to support a 15 MW turbine, modified from an NREL/IEA 15 MW turbine [2], for Korean offshore application. The original turbine designed for the semi platform was modified for the current TLP application.

Time domain simulations were conducted on the parked turbine, considering the site's extreme conditions over a period of 50 years. This paper presents the results of the concept design, including the basis of design, platform configuration, and system identification. An extreme response analysis was conducted for intact and damaged tendons, wave variations, heading variations, and water level changes. The designs are confirmed to comply with the design criteria from the industry standards DNV [20], API [21], and offshore platform design practices.

## 2. Basis of Design

### *2.1. Site and Metocean Conditions*

Figure 1 depicts a site located at 60 km east offshore from Ulsan City in South Korea. A constant water depth of 137 m is selected for the present design of the platform, although uneven bathymetry is observed around the target site.

The present design considered 50 yr extreme conditions to investigate the extreme responses of the platform and verify the strength of the design when subjected to typhoon sea conditions. Therefore, only parked turbine conditions were considered for the present concept design.

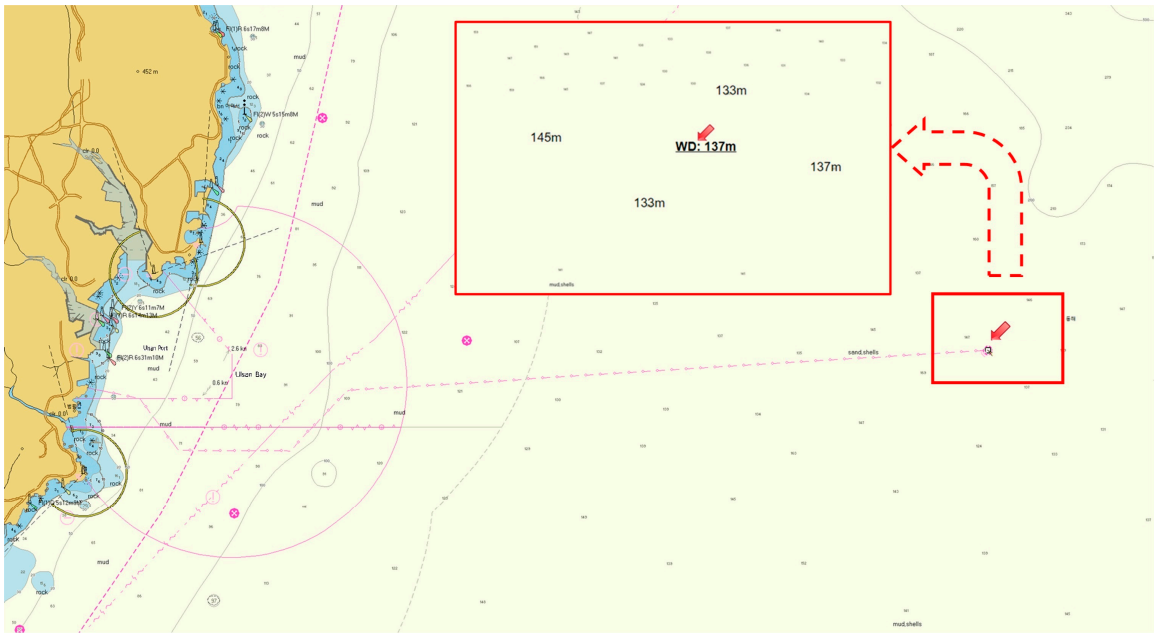


**Figure 1.** Target Site location and water depth.

Table 1 summarizes the 50 yr extreme conditions of the ultimate limit state (ULS) for wind, wave, current, and water levels [22]. The wind speed is a 1 h min average at 10 m above mean sea level (MSL), unless otherwise specified. For wave levels, the JONSWAP spectrum was used, represented by significant wave height Hs, spectral peak period Tp, and peak enhancement factor $\gamma$.

**Table 1.** The 50 yr extreme conditions for ULS.

| Description | Value |
|---|---|
| Wind: 1h mean, U10 [m/s] | 32.1 |
| Wave: Hs, [m] | 11.8 |
| Tp, [s] | 16.1 |
| $\gamma$, [-] | 2.5 |
| Current: surface/middle/bottom, [m/s] | 0.79/0.76/0.72 |
| Water level: tide/storm surge, [m] | 0.33/1.01 |

## 2.2. Design Criteria

The present TLP wind platform was designed to comply with the criteria summarized in [22] based on DNV [20], API [21], and offshore platform design practices. The platform global performance criteria in acceleration, pitch, and airgap are summarized in Table 2. Additionally, the platform natural frequencies of heave, roll, and pitch shall not exceed 6 s. The tendon was designed for the load factors from DNV [20]. The load factors in Table 3 are for the Consequence Class 2, as the present platform has redundant mooring (tendon) lines. Tendon tension utilization ratio (UR) for the tendon intact and damage conditions complies with a requirement, UR > 0.

**Table 2.** Platform global performance criteria.

| Parameters | ULS |
|---|---|
| Nacelle acceleration max, [m/s$^2$] | <5.0 |
| Platform pitch angle max, [deg.] | <5.0 |
| Airgap min, [m] | ≥1.0 |
| Platform natural frequency: heave, roll and pitch, [s] | ≤6.0 |

**Table 3.** Load factors for tendon design.

| Limit State | Mean, $\gamma_{mean}$ | Dynamic, $\gamma_{dynamic}$ |
|---|---|---|
| ULS | 1.3 | 1.75 |
| ALS intact | 1.0 | 1.1 |
| ALS damage | 1.0 | 1.25 |

In addition, minimum tendon tension at the anchor shall be positive for the ULS and ALS conditions to prevent a tendon slack.

The tension and design criteria for the tendon are defined as follows:

$$T_d = \gamma_{mean} T_{mean} + \gamma_{dyanamic} T_{dynamic} \quad (1)$$

$$S_c > T_d, \quad (2)$$

where $T_d$: tendon design tension, $\gamma_{mean}$: load factor for mean load, $\gamma_{dynamic}$: load factor for dynamic load, $T_{mean}$: characteristic mean tension, $T_{dynamic}$: characteristic dynamic tension, and $S_c$: characteristic capacity of the tendon line. Equations (1) and (2) lead the utilization ratio (UR) as

$$UR > 1.0, \quad (3)$$

where, $UR = S_c / T_d$.

## 3. TLP-Type Wind Platform Design

### 3.1. 15 MW Turbines

The NREL/IEA 15 MW developed for a semi-submersible platform [2] was modified for the TLP application. The resulting component weights and properties of the rotor, nacelle, and tower are summarized in Table 4, where the positive $x_{cg}$ and $z_{cg}$ directions are in the downwind direction and above the tower base, respectively. The moments of inertia for the components associated with dimension changes are omitted from the table.

**Table 4.** A 15 MW turbine system modified for TLP application.

| Description | Value |
|---|---|
| Power rate, [MW] | 15 |
| Rotor diameter, [m] | 240.0 |
| Tower height above base, [m] | 129.54 |
| Tower diameter at base/top, [m] | 9.5/6.5 |
| Hub height above base, [m] | 135.0 |
| Rotor + hub mass, [ton] | 274.9 |
| Nacelle mass, [ton] | 675.2 |
| Tower mass, [ton] | 1476.2 |
| Total mass, [ton] | 2426.3 |
| Mass center above tower base (Xcg, Ycg, Zcg), [m] | (−2.9, 0, 82.9) |

### 3.2. In-Place Platform Configuration

The 15 MW TLP-type platform (KRISO-TLP) properties are summarized in Table 5, which is configured following several design iterations until the design compliances are verified, especially regarding wet-tow stability, minimum tendon tension, and tendon strength. The details of the design iterations are not reported in this paper.

**Table 5.** In-place 15 MW TLP wind platform particulars.

| Description | Value |
|---|---|
| Displacement, [ton] | 11,846.6 |
| Draft, [m] | 18 |
| Hub height above MSL, [m] | 150 |
| Length overall, [m] | 85.11 |
| Center column diameter, [m] | 10 |
| Center column height, [m] | 33 |
| Outer column height, [m] | 28 |
| Outer column square width, [m] | 11.5 |
| Pontoon width × depth, [m] | 7.5 × 4.5 |
| Deck width × depth, [m] | 4 × 3 |
| Turbine mass, [ton] | 2426.3 |
| Hull steel and ballast mass, [ton] | 3415.7 |
| Total mass, [ton] | 7344.7 |
| Mass center, CoG (Xcg, Ycg, Zcg), [m] | (−1.04, 0, 9.34) |

The platform consists of the center column to mount the turbine, pontoons, outer columns, and deck structures connecting the columns. The outer column has a square section to facilitate its fabrication. The platform displacement is about 11,847 tons at the operation draft of 18 m. The platform mass center is at (Xcg, Ycg, Zcg) = (−1.04, 0.0, 9.34) m, for which the reference coordinate is defined in the following section. The hub height is 150 m above the sea level. Lightships with the integrated turbine has a displacement of 5842 tons with a draft of 5.7 m. The metacentric height of its GM is 11.4 m, which confirms that the lightship is stable. A wet-tow displacement at a 10 m draft is 7950 tons, and its GM is about 9.7 m, demonstrating self-stability during the tow operation.

Table 6 summarizes the tendon properties. The platform is vertically moored with a total of nine tendons with a group of three per each outer column. A steel wire rope with 141 mm is used for the tendons. Pretension on each tendon is about 27.8% of the minimum breaking load (MBL) of the tendon. Number of tendons, tendon size, and pretension are based on the design iterations described above.

**Table 6.** Tendon system for 15 MW platform.

| Description | Value |
|---|---|
| Number of tendons, [-] | 9 |
| Tendon length each, [m] | 119 |
| Tendon (wire rope) diameter, [mm] | 141 |
| Axial stiffness, [kN] | $1.8 \times 10^6$ |
| MBL, [kN] | 19,180 |

Figure 2 illustrates the layout of the platform, tendons, and driven pile anchors. Three tendons per each outer column are used. The one end of the tendon is connected to the outside bottom of the outer column, and the other end is tied to the top of the driven pile. Although there are pros and cons for the driven pile, it is used due to its technological suitability for offshore TLP anchoring. There may be alternative options of a gravity anchor or suction anchor, but those are beyond the scope of the present study. The driven pile is designed such that sufficient vertical holding capacity with soil penetration depth is maintained and stick-up height above the seabed is provided for the pile driving hammer, but its design details are excluded from this paper.

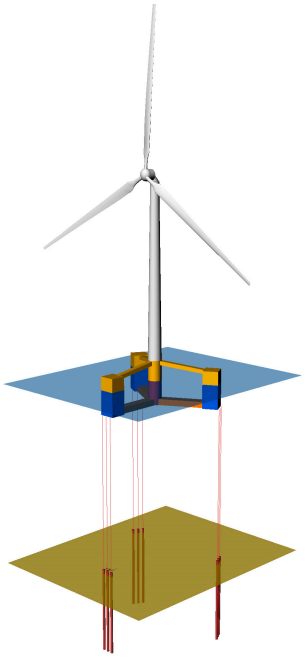

**Figure 2.** KRISO-TLP platform layout presenting TLP hull, tendons, and anchors.

## 4. Analysis Modeling

A coordinate system is defined in Figure 3. The reference origin is located at the platform center on mean sea level (MSL). Heading definition is also provided, such that the headings of 0 deg and 90 deg are aligned toward the positive x- and y-directions, respectively. For the present layout, the platform's north (y-direction) is aligned with true north. The depicted tendons, numbered from T1 to T9, are grouped in threes: northeast (T1–T3), southeast (T4–T5), and west group (T7–T9). Tendon separation between the adjacent tendons is properly chosen to prevent interference between the piles during pile installation.

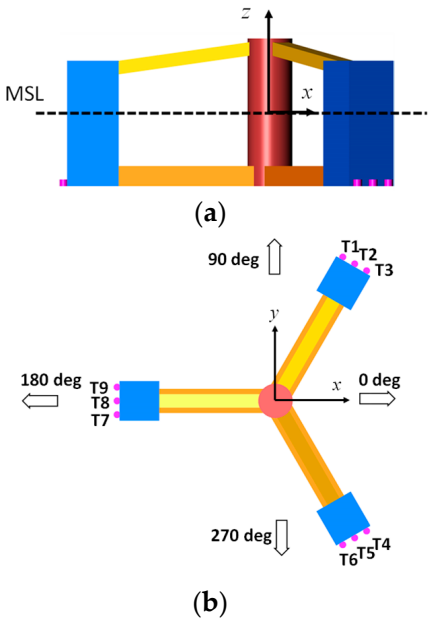


**Figure 3.** Reference coordinate system: (**a**) Coordinate system; (**b**) heading definition, tendon group and numbering.

### 4.1. Turbine System Modeling

The turbine system is considered a rigid body, such that the hull and turbine are modeled as a single rigid body. Therefore, the couplings of the turbine with the platform mooring are ignored in the present analysis, and thus the analysis of the operating conditions is excluded. This approach can facilitate and expedite the extreme response analysis for the present concept design with minimal involvement of complex coupling with the turbine.

### 4.2. Drag and Hull Viscous Damping Modeling

Wind drag force acting on the structure exposed to air and current drag on the submerged hull can be computed using the following equation:

$$F_{drag} = \frac{1}{2}\rho C_d A V^2, \tag{4}$$

where $F_{drag}$ = wind or current drag force, $\rho$ = mass density of air or water, $C_d$ = drag coefficient, $A$ = projected area to the wind or current direction, and $V$ = wind or current velocity. The used drag coefficients are shown in Table 7. Here, the wind drag induced by the tower and nacelle are included in the analysis. Those are estimated using [23]. Platform hull viscous damping is implemented in terms of Morrison components. The Morrison elements of the outer and center columns are extended to the top of those structures to capture the fluid velocity variations below the instantaneous water surface.

**Table 7.** Drag coefficients.

| Structure | Normal | Vertical |
|---|---|---|
| Outer Column | 2.2 | 1.4 |
| Center Column | 1.0 | 1.1 |
| Pontoon | 1.8 | 2.4 |
| Deck | 2.0. | - |
| Tower | 1.0 | - |
| Nacelle | 1.0 | - |
| Tendon | 1.2 | - |

### 4.3. Time Domain Simulation

The dynamic response analysis was conducted in the time domain of 50-year extreme (parked) conditions. The simulation includes the first-order and second-order low-frequency effects with hydrodynamic coefficients. The analysis excludes the second-order sum frequency effects [6,24]. The wind and current drag forces are computed at each time step considering the relative velocities between the flow and platform motion in the numerical simulation. Numerical modeling and simulations are conducted using Orcaflex [25].

### 4.4. Extreme Value Analysis

A single three-hour time domain simulation excluding the initial transient responses is used for the extreme value analysis.

The extreme values for the responses may be calculated using the following equation:

$$R_{extreme} = R_{mean} + 2\sigma_R \times \left[-0.5\ln\left(1 - p^{1/N}\right)\right]^{1/2}, \tag{5}$$

where $R_{extrme}$, $R_{mean}$, $\sigma_R$, and $p$ are the extreme response, mean response, standard deviation of the response, and probability, respectively. N is the number of cycles from the 3 h time domain simulation. The response at the 90% percentile level is taken as an extreme (maximum) value, based on the recommendation of [23]. The extreme responses (motion, acceleration, tension, airgap, etc.) in Equation (5) were used for the analysis in Section 6.

Dynamic amplification factor (DAF) of the tendon tension can be given as follows:

$$DAF = T_{extreme}/T_{pretension}, \quad (6)$$

where $T_{extreme}$ and $T_{pretension}$ are the extreme tendon tension and tendon pretension. The pretension, $T_{pretension}$ is an averaged pretension at static equilibrium with no environment applied, as described in Section 5.1.

## 5. System Identifications

### 5.1. Tendon Tension at Static Equilibrium

Figure 4 shows each tendon pretension ratio to the pretension averaged ($T_{pretension}$), for the tendon intact condition without the environment loads. Platform static displacements in the surge and pitch at the static equilibrium are −0.004 m and −0.013 deg due to the platform mass center eccentricity in the negative x-direction. Therefore, the tendons in the northeast (NE) and southeast (SE) groups are tauter than those in the west group, resulting in unidentical pretensions across tensons at the static status. Therefore, it is observed that the NE and SE group tendons take about 5% more loads than those in the west group. The averaged pretension from this section is used in Section 6.

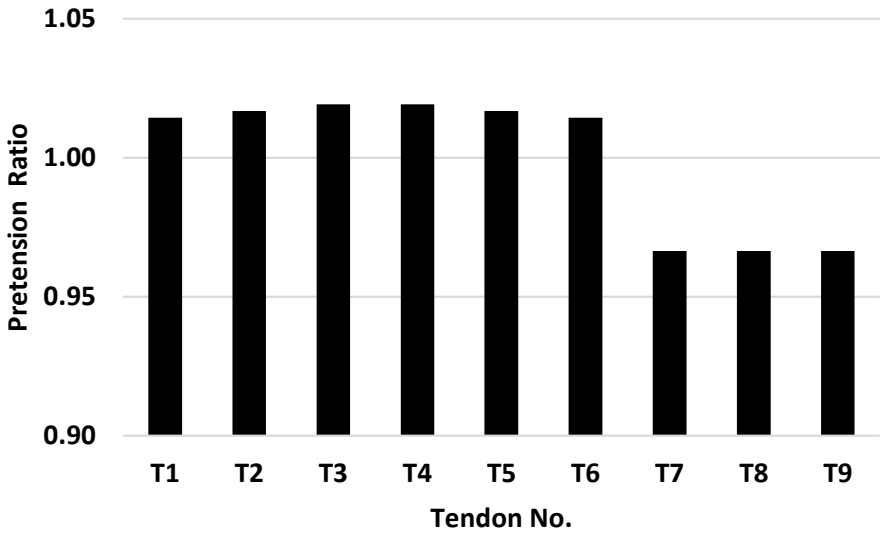


**Figure 4.** Tendon pretension ratio to the average pretension at static equilibrium.

### 5.2. Offset, Setdown, and Restoring Force

When TLP is statistically displaced to a location, the platform is pulled down (setdown) due to the tendon force.

Figure 5 depicts setdowns and system restoring forces associated with the offsets. Figure 5a shows that a setdown of 2 m occurs when the platform is statically displaces about 18% of the water depth in the x- or y-directions. Figure 5b presents the surge and sway restoring forces induced by the offsets in the x- and y-directions, where the restoring force is normalized by $T_{pretension}$.

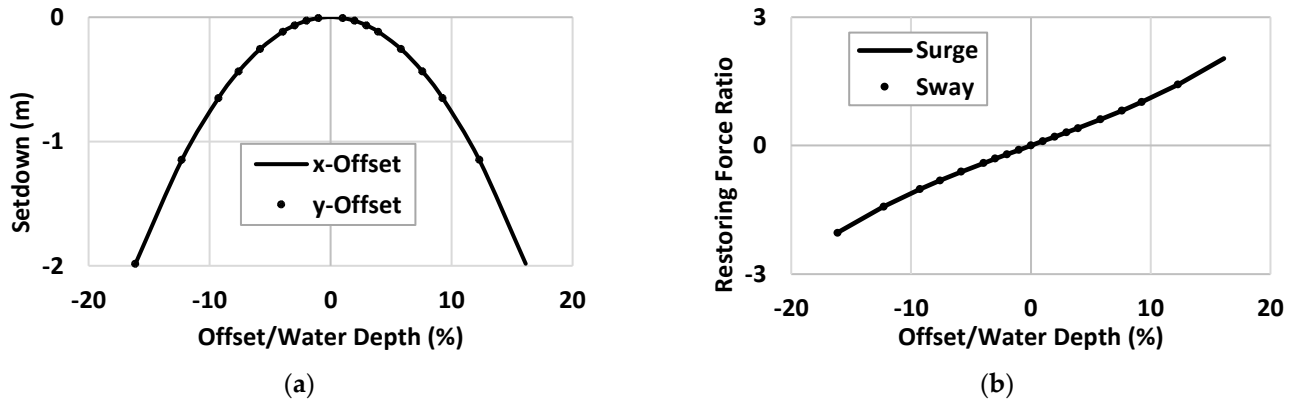


**Figure 5.** Curves for the setdown and restoring force ratio: (**a**) offset vs. setdown; (**b**) offset vs. restoring force.

Figure 6 presents the surge stiffness calculated using the restoring force curve. Linear surge stiffness can be found at a very small offset. This result indicates that the surge stiffness becomes highly nonlinear even at a small offset ratio. and its nonlinear tendency increases with the offset increase.

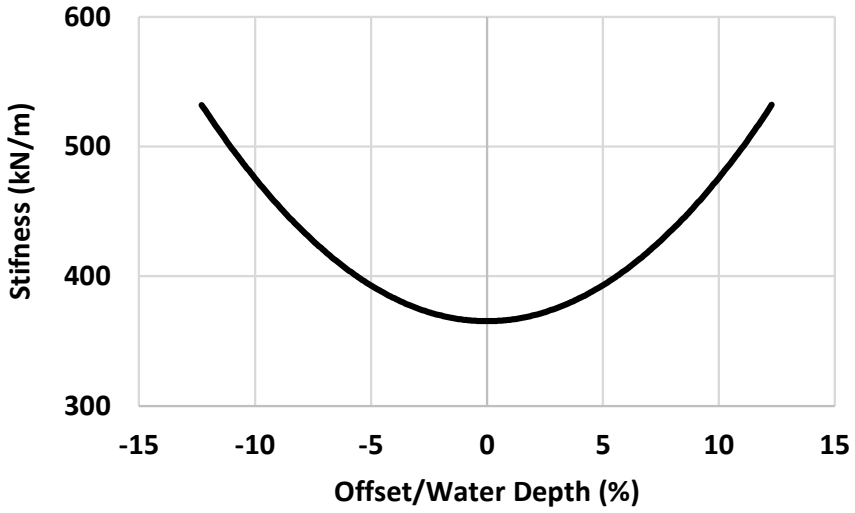


**Figure 6.** Stiffness curve of the tendon system in the surge direction.

### *5.3. Offset Due to Wind and Current Forces*

Wind and current drag forces can cause the platform to offset downward in the flow direction. The x-offset ratios to the water depth (WD) induced by those forces are shown in Figure 7. Under 50 yr extreme conditions, the 1 h wind at 10 m above sea level and the surface current are about 32 m/s and 0.8 m/s (Table 1). Therefore, platform static offset due to the wind and current under extreme conditions will be about 3.2% and 1.3% of the water depth, respectively. The results indicate that the wind drag induces more horizontal displacement of the platform than the current drag at the 50 yr sea states.

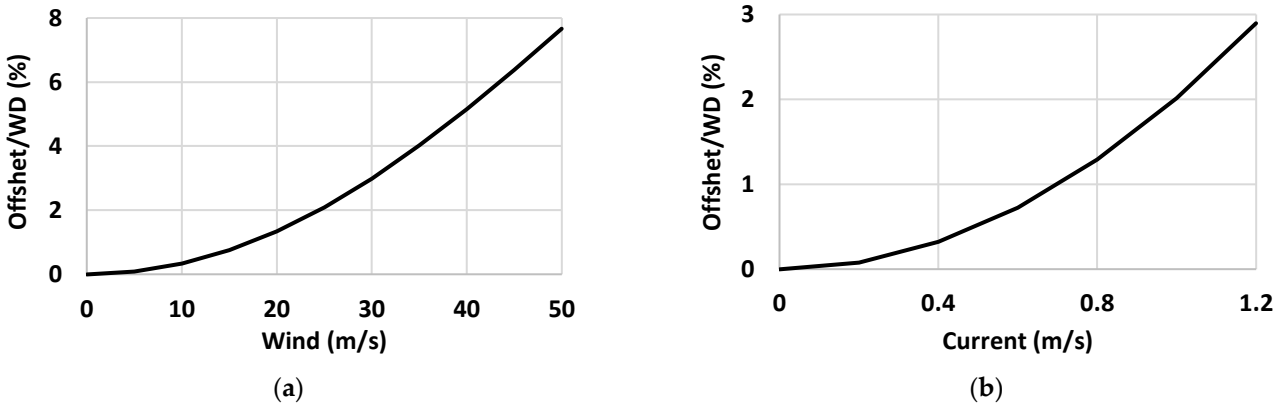


(a) (b)

**Figure 7.** Platform static x-offset ratios due to wind and current: (**a**) platform offset induced by wind; (**b**) platform offset induced by current.

### 5.4. Decay Test and Natural Period

Natural periods (frequencies) for platforms estimated from the decay tests are shown in Table 8. The roll and pitch natural periods are well below the allowable maximum of 5 deg, confirming the design compliance, as shown in Table 2. Note that the result is for the present modeling with no coupling of the flexible tower. According to our preliminary analysis with the flexible tower (excluded in this paper), the pitch natural frequency of the platform shifted to a lower frequency toward the lowest eigen frequency of the tower. The pitch frequency shift is also reported in the mono-column TLP wind analysis [6]. Therefore, the platform pitch frequency is suggested to be further evaluated considering the flexibility of the tower in the future.

**Table 8.** Platform natural period.

| Motion | Period (Frequency) |
|---|---|
| Surge, [s] ([Hz]) | 43.13 (0.023) |
| Sway, [s] ([Hz]) | 43.21 (0.023) |
| Heave, [s] ([Hz]) | 2.09 (0.478) |
| Roll, [s] ([Hz]) | 3.15 (0.317) |
| Pitch, [s] ([Hz]) | 3.15 (0.317) |
| Yaw, [s] ([Hz]) | 31.27 (0.032) |

The critical damping ratio $\zeta$ can be estimated using the logarithmic decrement given as follows:

$$\zeta = \frac{1}{2n\pi} ln \frac{x_i}{x_{i+n}} \quad (7)$$

where $x_i$ and $x_{i+n}$ are the amplitude peaks of the oscillations at the $i$th and $(i+n)$th oscillation peaks, and $n$ is the number of the oscillations.

Figure 8 presents the decay time histories of the motions and exponential fit of the linear damping for the decay motions. For the present damping estimate, the initial and seventh amplitude peaks are used. The exponential decays (envelopes) in heave, roll and yaw present a good fit to the decay maxima and minima, showing that the estimated linear damping ratios work well for those motions. The surge, sway, and pitch envelopes show some differences in the initial few oscillations, which may be caused by nonlinear damping. Pitch damping is shown to be higher than roll damping. Irregular oscillations are presented in the pitch decay, and its decay patterns are different from those of the roll decay. This is mainly due to the coupling of the eccentricity of the platform mass center as no flexible tower is modeled in the analysis. Therefore, care should be taken for the pitch damping estimate of a TLP, especially with a flexible tower, because severe irregularities in the pitch decay pattern due to the tower flexibility and tendon stiffness were observed from our preliminary analysis and in [17].

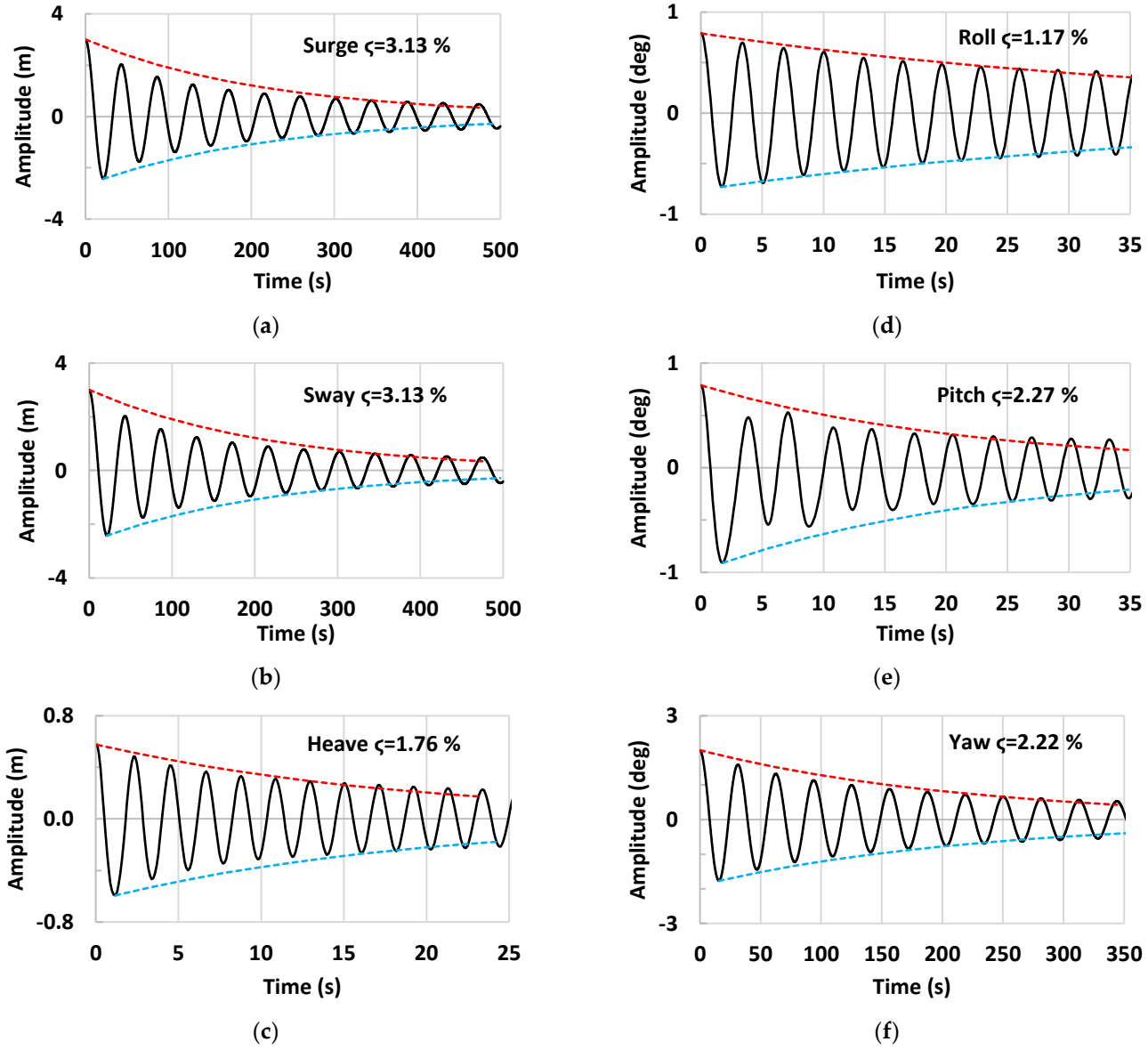


**Figure 8.** Time histories from decay simulations of the platform: (**a**) surge; (**b**) sway; (**c**) heave; (**d**) roll; (**e**) pitch; (**f**) yaw. The red and blue dotted lines indicate the exponential decay envelops.

### *5.5. Response Amplitude Operators*

White noise waves with Hs = 2 m were used to compute the response amplitude operators (RAOs) for the wave heading 0 deg. The RAOs of the motions, accelerations at the nacelle location, and tendon tensions are shown in Figure 9. The spectral peak frequencies of the surge, heave, and pitch motions capture the natural motion frequencies, as shown in Table 8. The horizontal (x-direction) and vertical (z-direction) peak frequencies correspond to the pitch and heave frequencies, respectively. It is seen that the horizontal acceleration of RAOs is much greater than their vertical acceleration.

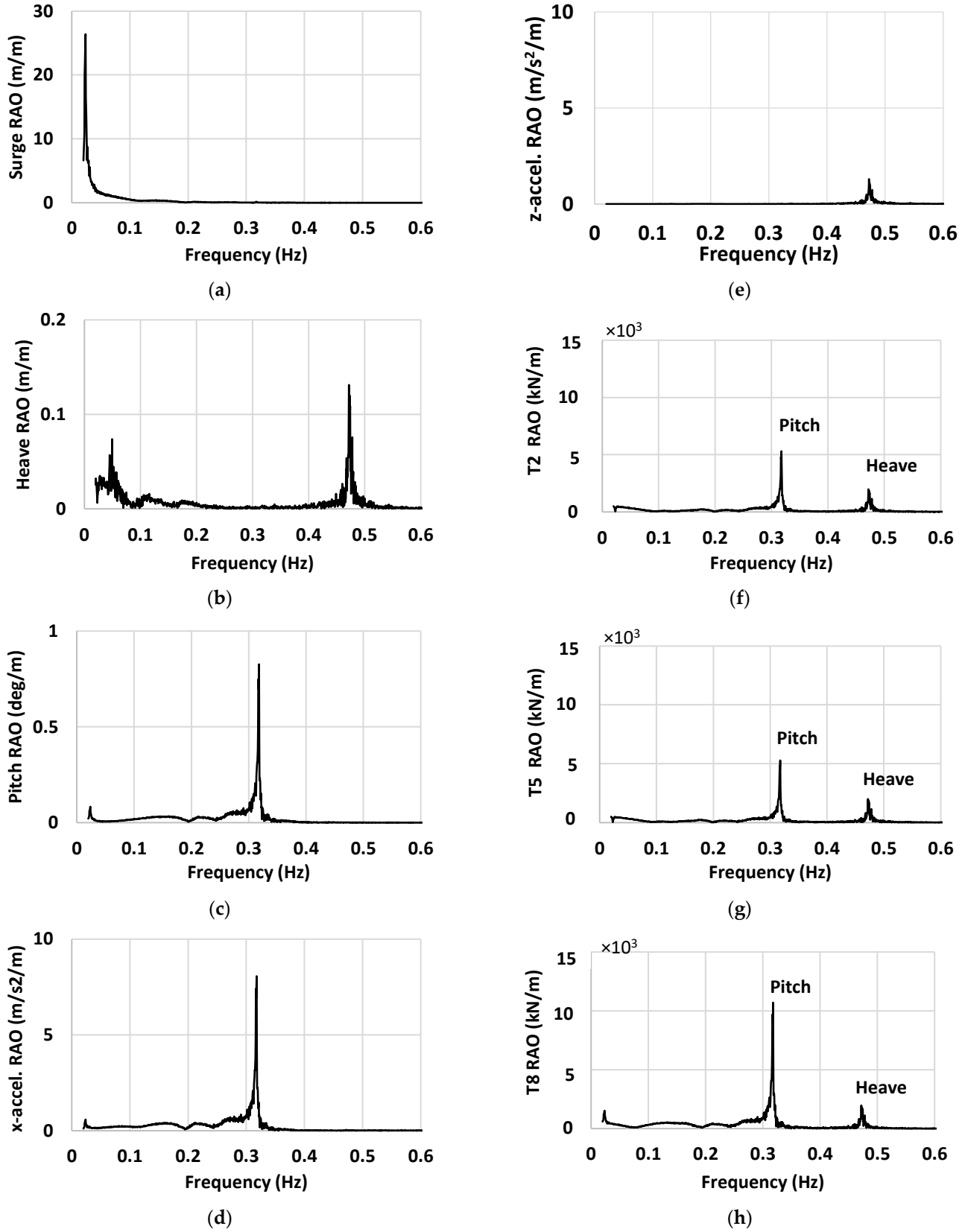


**Figure 9.** RAOs of platform motion, nacelle acceleration, and tendon tension: (**a**) surge; (**b**) heave; (**c**) pitch; (**d**) x-accel. at nacelle; (**e**) z-accel. at nacelle; (**f**) T2 tension; (**g**) T5 tension; (**h**) T8 tension.

For the tendon tension RAOs, the middle tendons of T2, T5, and T8, among the tendons in each tendon group, are selected, as the tendons in the same group take almost the same loads due to their close spacing (Figure 3). In the present wave heading of 0 deg, it is observed that the tendons in the weatherside tendon group (T7, T8, T9) are affected more than those in the leeside tendon groups (T1~T6) due to the platform pitch-coupled effects. A stronger coupling effect with the pitch compared to the heave is also presented in tension RAOs.

## 6. Analysis Result and Discussion

### 6.1. Wave Condition Variation

Present analysis considers a condition of 50-yr extreme, turbine parked condition, DLC 6.1 [26]. The waves, Hs and Tp, as shown in Table 2, are for a single joint wave under 50 yr extreme conditions, instead of the environmental (Hs, Tp) contour of extreme values from the IFORM contour approach [23,27]. Therefore, it may suggest that additional wave conditions are considered to cover the additional waves with Hs and Tp variations. Load cases (LCs), as shown in Table 9, are constructed for these purposes.

**Table 9.** Load cases (LCs) with Hs and Tp variation.

| LC | Hs [m] | Tp [s] | Ratio from Base Case Hs, Tp |
|---|---|---|---|
| LC1 | 11.21 | 14.35 | 0.95 Hs, 0.95 Tp |
| LC2 | 11.21 | 15.10 | 0.95 Hs, Tp |
| LC3 | 11.21 | 15.86 | 0.95 Hs, 1.05 Tp |
| LC4 | 11.8 | 14.35 | Hs, 0.95 Tp |
| LC0 | 11.8 | 15.10 | Hs, Tp (base case) |
| LC5 | 11.8 | 15.86 | Hs, 1.05 Tp |
| LC6 | 12.39 | 14.35 | 1.05 Hs, 0.95 Tp |
| LC7 | 12.39 | 15.10 | 1.05 Hs, Tp |
| LC8 | 12.39 | 15.86 | 1.05 Hs, 1.05 Tp |

The base case (LC0) is the environmental condition with the waves Hs and Tp, as shown in Table 2. Other LCs are for the variations of Hs and Tp, ± 5% increase compred to the base case for Hs and Tp. For example, 0.95 Hs or 1.05 Tp indicates 5% decrease in Hs from the LC0 or 5% increase in Tp from the LC0. The same wind and current, as shown in Table 2, are used for all the LCs. The Norwegian Petroleum Directorate (NPD) wind spectrum is used for 50-year wind generation. Both tendon intact and damage conditions are considered for the LCs. The environments of wind, wave, and current levels are assumed to have a co-directional heading of 0 deg for the present analysis, unless mentioned otherwise. Under this heading, according to the prescreening analysis, the west tendon group (T7, T8, and T9), as shown in Figure 2, is identified as the most loaded tendon group. Therefore, among the west tendon group, T9 is considered a damage tendon for the tendon damage case, based on [21].

#### 6.1.1. Platform Motions

Figure 10 compares the platform maximum offset ratio to the water depth for the LCs with the tendon intact and with T9 damage. Note that the LC0 (base case) is placed in the middle of the horizontal axis for easy comparison with other LCs. Higher offsets occur under higher wave heights (LC6-LC8), and shorter Tp (LC1, LC4, LC6) among the same wave height group in the LCs. The offset criteria are not typically specified for the TLP wind platform design, but they can be investigated in terms of the power cable design, tendon angle at the anchor and airgap. The offsets for the cases of intact and damaged tendon show no noticeable differences. The maximum offset ratio is below 20%. This offset ratio may be within an acceptable range for the dynamic power cable design, which is a future variable to be identified.

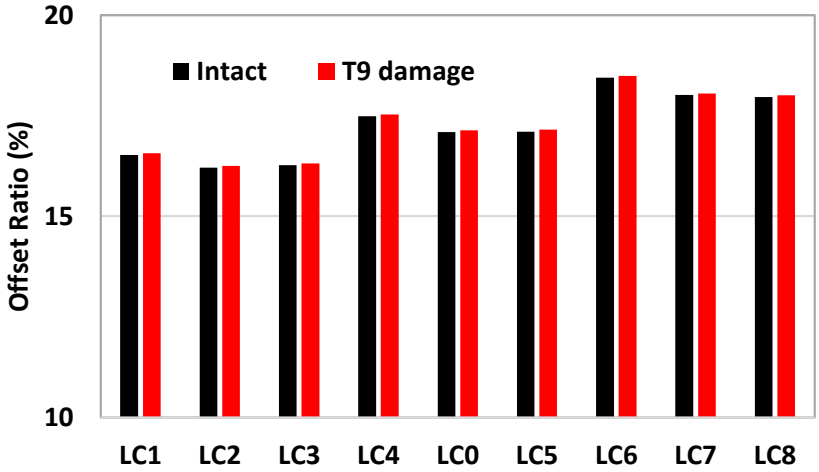


**Figure 10.** Platform maximum offset ratio to water depth for intact tendon and tendon with T9 damage.

Figure 11 shows the maximum tendon angles from the vertical axis (0 deg for the upward direction) at the anchor for the intact tendon condition due to the offsets in Figure 10. According to API [21], it is recommended that the tendon angle at the anchor does not exceed the angle (typically 10 deg) for the conventional tendon fabricated with steel tubulars used for the offshore TLP. This prevents the tendon and bottom connector from colliding with the tendon pile anchor. However, the present tendon is a wire tendon and the considered tendon connector is a simple connector and different from the conventional TLP connector. Therefore, the tendon angle constraints can be removed as long as there is no design issue with the power cable (with the offsets presented in Figure 10) or airgap.

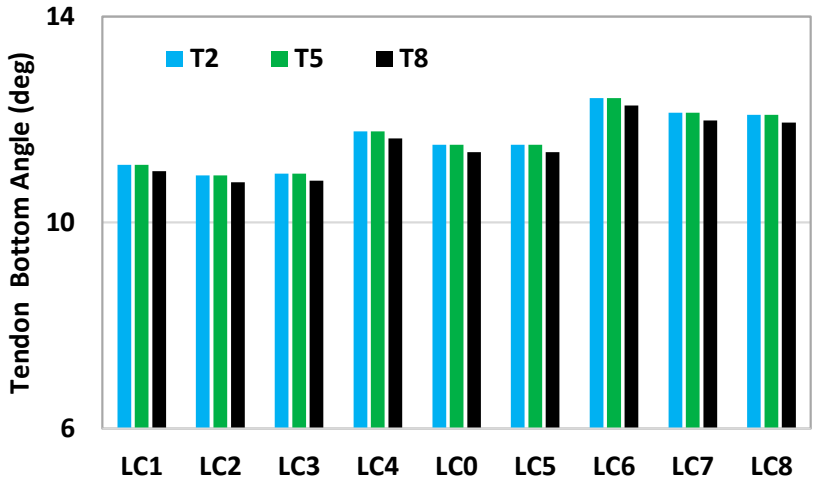


**Figure 11.** Tendon angle at anchor for intact tendon.

Figure 12 presents the maxima, minima, and mean value (dot mark) of the heave and pitch motions for the intact tendon condition. The maximum value trends of the motions are very similar to those of the offset results across the LCs. Maximum platform pitch is below 0.3 deg, which is much lower than the allowable maximum of 5.0 deg, as shown in Table 2.

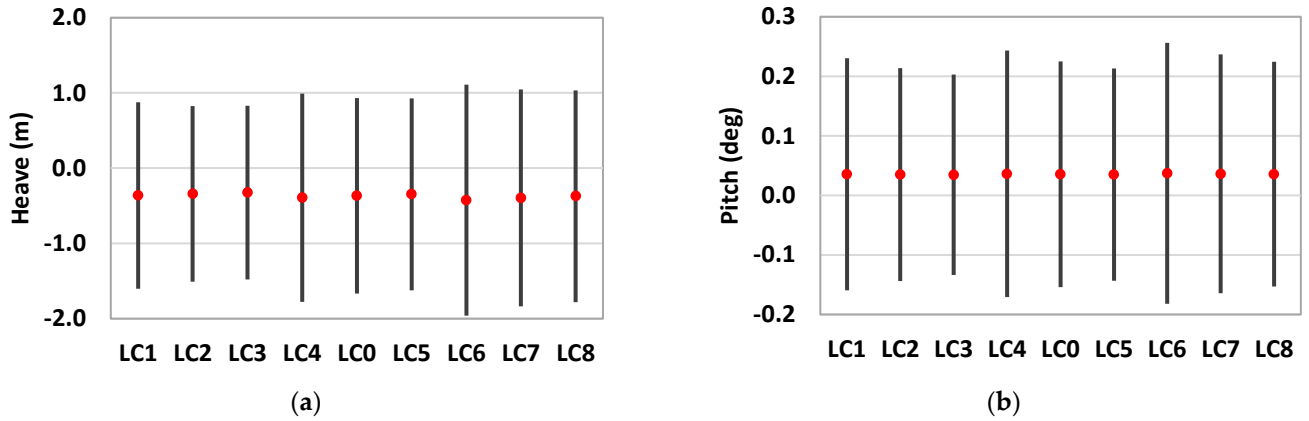


**Figure 12.** Platform motions for tendon intact: (**a**) heave; (**b**) pitch.

### 6.1.2. Nacelle Accelerations

Extreme (max) values of the accelerations at the nacelle height are compared in Figure 13. The horizontal accelerations are much greater than the vertical accelerations. The maximum acceleration at the nacelle is about 2.7 m/s$^2$, which is smaller than the design criteria of 6.0 m/s$^2$. Like the platform motion trends, the shorter period waves cause higher horizontal accelerations.

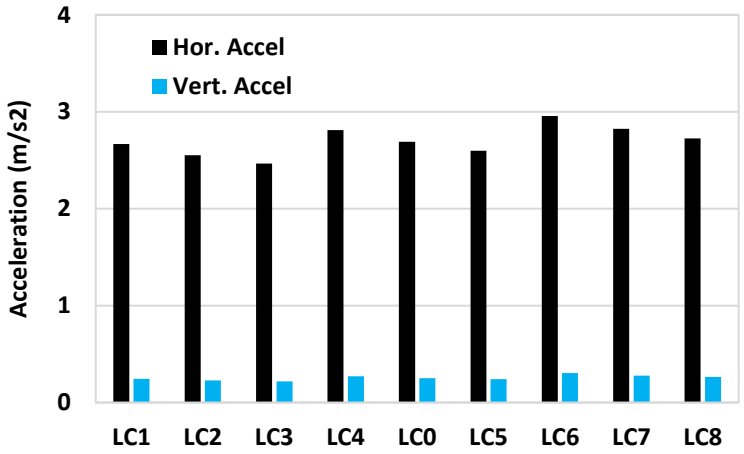


**Figure 13.** Accelerations at nacelle.

### 6.1.3. Airgap

There are two key structures for airgap evaluation: the center column and the deck. The airgap is a vertical distance above the instantaneous wave surface to the bottom of the targeted structure. For the present design phase, our interest is in the center column, as the turbine is mated at the top of the center column, and structural design issues or leaks due to waves may occur at the mating section.

Minimum airgap results on the center column are presented in Figure 14. The airgaps are smaller in the higher wave LCs (LC6, LC7, and LC8) as anticipated, which is associated with the wave height increase but a very small change in heave, as depicted in Figure 12. All airgaps are greater than the allowable minimum of 1.0 m, except for LC6, where the airgap marginally meets the criteria.

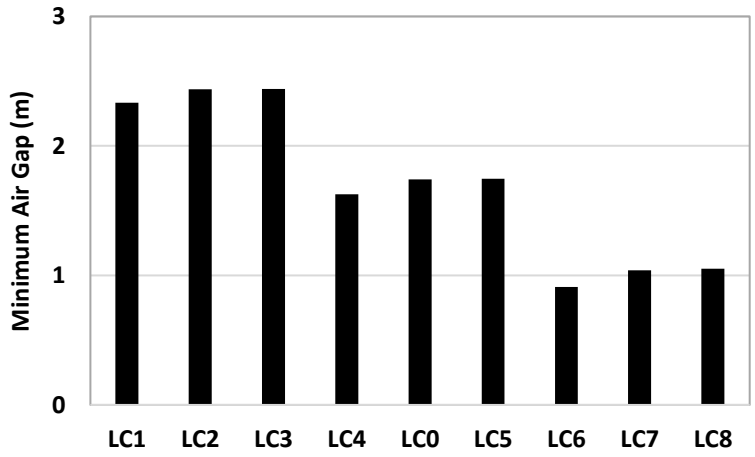


**Figure 14.** Minimum airgap to the tower base on the center column.

6.1.4. Maximum Tendon Tension

The maximum tendon tension on each tendon before and after T9 damage is evaluated for the base case LC0. For this, the middle tendons T2 and T5 in the intact tendon group and remaining tendons T7 and T8 in the damaged tendon group are selected. Each tendon tension for the damaged case ($T_{damage}$) is normalized by each intact tendon tension ($T_{intact}$). The resulting ratios ($T_{damage}/T_{intact}$) are presented in Figure 15. There is a significant tension increase in the damaged tendon to about 1.57 times the intact tension for T7 and T8, as T7 and T8 share dynamic loads due to the missing T9. Compared to those, the T2 and T5 tensions show a small variation in tension from the intact tendon. The result indicates that tendon damage highly affects the tension increase in the neighboring tendons in the damaged tendon group.

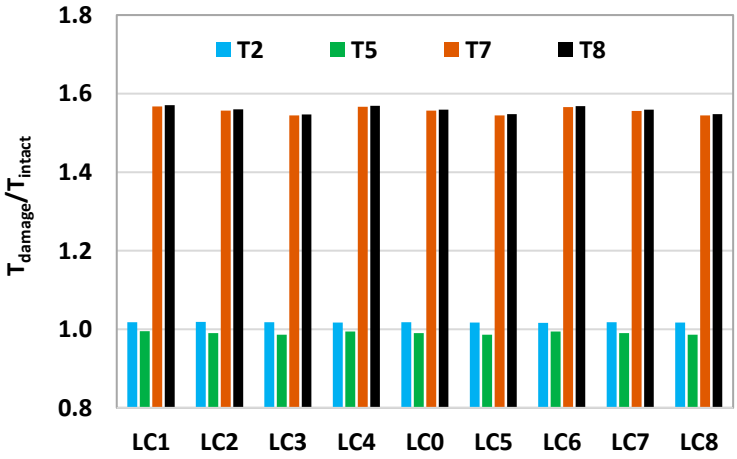


**Figure 15.** Maximum damaged tendon tension ratio to the intact tendon tension for LC0.

Among the 3 h simulation time histories, part of the T8 tensions before and after T9 damage are presented in Figure 16, capturing the highest peak tension around 6100 s. Here, the T8 tension is normalized by the averaged pretension ($T_{pretension}$) described in Section 5.1. It shows a mean tension shift between the damaged case and the intact case. The remaining T8 (and T7) experiences higher dynamic loads due to reduced tendon stiffness from the missing tendon. The standard deviation of T8 tension for the damaged case is 1.7 times larger than that for the intact case, which also indicates the higher dynamics in tension with the damaged tendon.

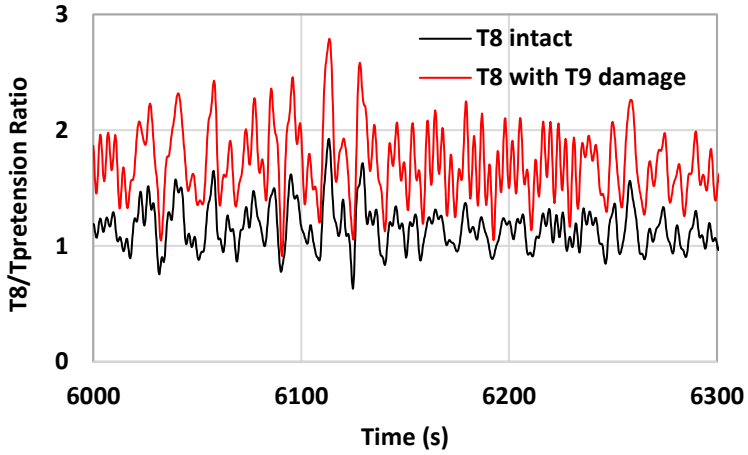


**Figure 16.** Time histories of T8 tension for intact and T9 damage cases for LC0.

The 3 h tension time histories (Figure 16) are further processed to compute the probability of exceedances of T8 tension. The resulting values for the intact and damaged tendon cases are compared in Figure 17. The results show a quite different probability of exceedance distribution. The tension ratio to the pretension ($T_{pretension}$) exceeding 10% probability is about 1.3 for the intact and 2.0 for the damage case, respectively.

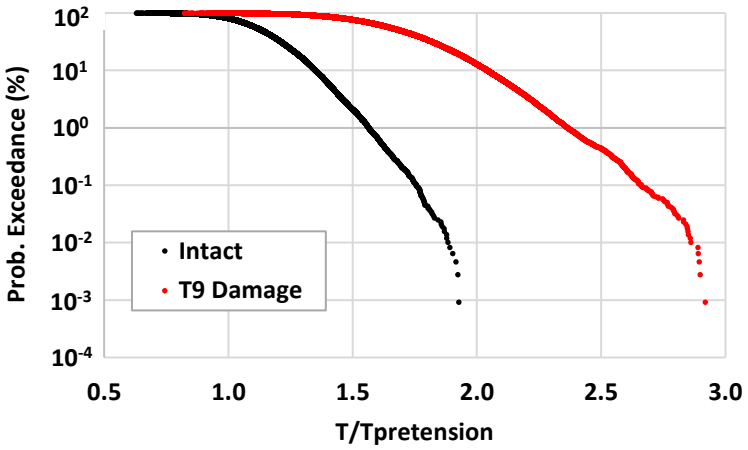


**Figure 17.** Probability of exceedance of T8 tension before and after T9 damage.

Figure 18 compares the power spectral density (PSD) of T8 before and after T9 damage. It shows a stronger contribution from the platform pitch motion in tensions than the heave motion. The peak spectral frequencies on the T8 tension for the intact condition are associated with the natural heave and pitch frequencies of the platform. The mooring (tendon) system stiffness with T9 damage is reduced by 11.1% for heave and 22.0% for pitch, compared to the intact system. Therefore, both peak frequencies caused by the heave and pitch for the T9 damage are shifted to lower frequencies, which indicates that the heave and pitch frequencies of the platform are closer to the wave energy frequencies. Therefore, the platform with the damaged tendon may be susceptible to take more excitation energies from the waves, which may result in additional damage to the tendon system or platform structures.

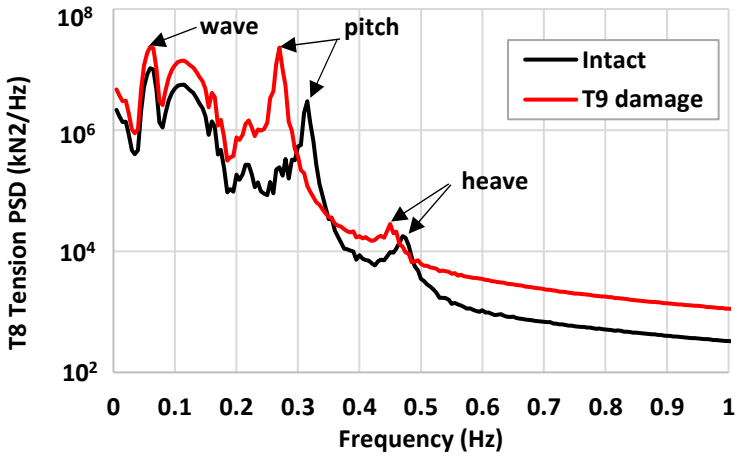


**Figure 18.** T8 tension PSD for intact and T9 damage cases for LC0.

Extreme (maximum) tension URs at the tendon top for the intact and damaged tendon cases are shown in Figure 19. The weatherside (west) tendon group (T7~T9) have lower URs than those in the leeside tendon groups. The lowest UR is about 1.7 for the intact and 1.2 for the tendon damage conditions, respectively. The analysis results show that all UR values for the intact and damaged tendon cases exceed the allowable minimum of 1.0, confirming the compliance of the tendon strength design.

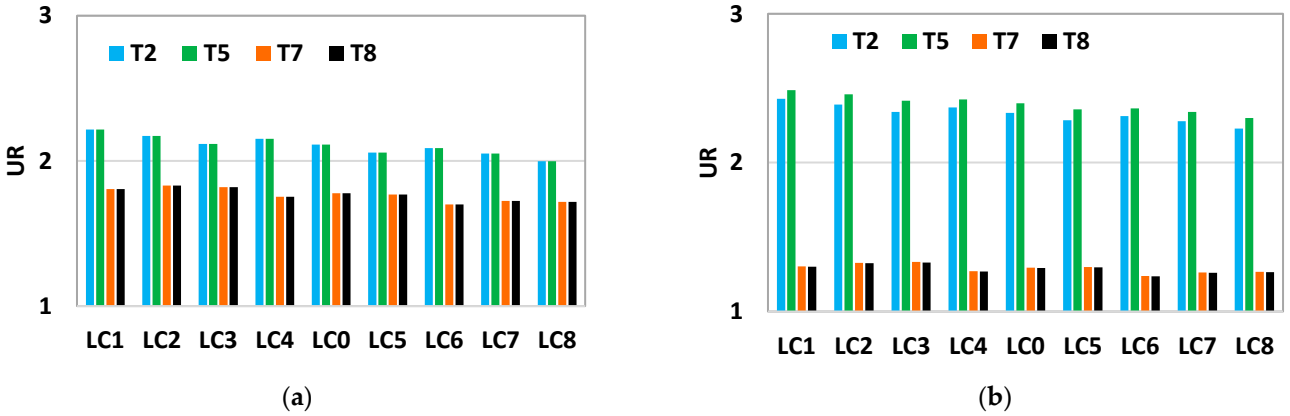


**Figure 19.** UR of the extreme tensions for intact and T9 damage cases: (**a**) tendon intact; (**b**) T9 damage.

Tendon tension DAF values are compared in Figure 20. The DAF values for the intact and damaged cases are calculated using the pretension ($T_{pretension}$). Higher DAFs are observed in the higher or shorter waves, which are related to the platform motions presented in Figures 10 and 12. Average DAF for the intact tendon (Figure 20a) is about 1.86 for the weatherside (west group) and 1.57 for the leeside tendons (northeast and southeast groups). Due to the damaged tendon T9, the DAFs for the T7 and T8 are nearly three times the averaged pretension, which is quite a bit of amplification.

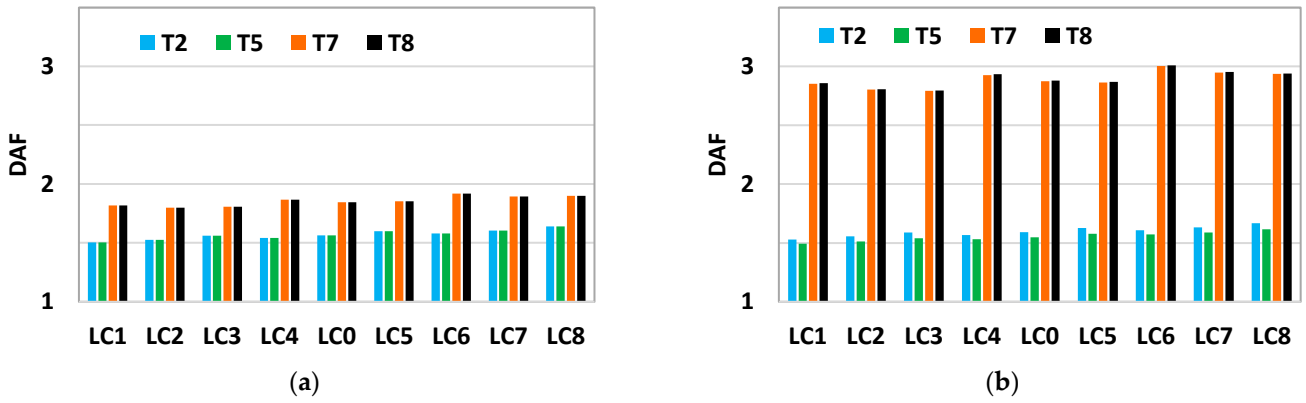


**Figure 20.** Tendon tension DAF for intact and T9 damage cases: (**a**) intact tendon; (**b**) T9 damage.

Tendon tensions due to heading variations at every 15 deg from 0 deg to 180 deg were further investigated for the base case (LC0) environment and tendon intact case. The resulting maximum tension ratios at each heading are shown in Figure 21, where the tension ratio is the max tensions of T2, T5, and T8 divided by the max tension of T8 at the heading 0 deg. The tendon number with the maximum tension at each heading is presented at the top of each bar chart. Other headings from 180 deg to 360 deg are excluded due to symmetricity of the tendon layout. The largest tension occurs at the heading 120 deg, while the lowest tension occurs at 60 deg or 180 deg. Tension variations are in the range from −8% to +2% from the tension at 0 deg. The results suggest that the installed platform is properly oriented in the direction that lowers the extreme tensions.

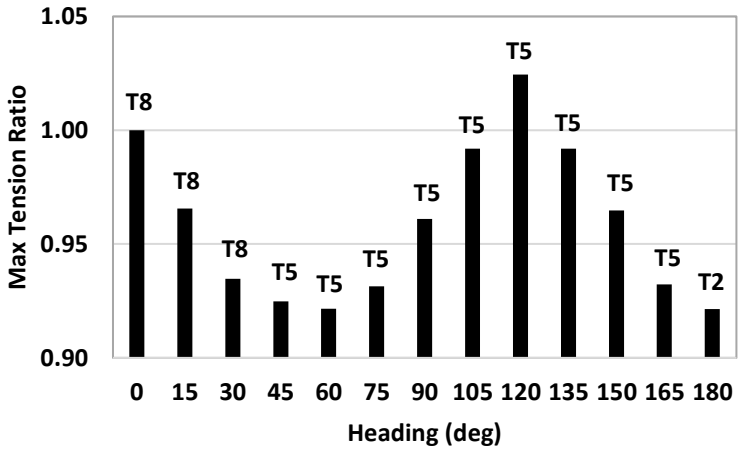


**Figure 21.** Maximum tension ratio to T8 tension at 0 deg (LC0 and tendon intact case).

### 6.1.5. Minimum Tendon Tension

The base case LC0 is considered for the evaluation of the minimum tendon tension at anchor (tendon bottom). Minimum tensions on T1 to T9 before and after T9 damage are normalized by the pretension ($T_{pretension}$) for the intact case, and the resulting ratios are compared in Figure 22. The tendon damage affects the minimum tensions across the tendons. Tensions on some leeside tendons (T3, T4 and T5) after damage are reduced from those that are intact. The lowest anchor tension due to T9 damage occurs on T4, which is about 31% of $T_{pretension}$, confirming the compliance with the allowable minimum tension requirement.

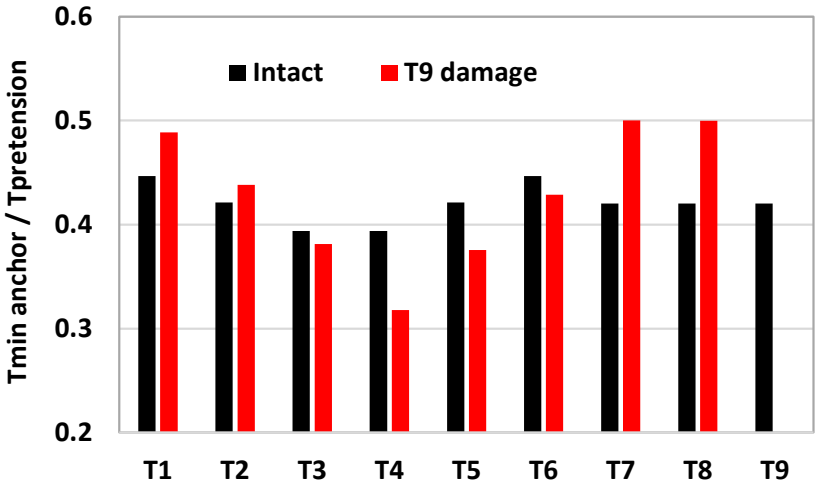


**Figure 22.** Minimum tension ratio at anchor to $T_{pretension}$ (LC0).

### *6.2. Wave Level Variation*

#### 6.2.1. Platform Motions

Water levels vary from −1.0 m to +1.0 m from the base case level of MSL (Table 1) with an increment of 0.2 m~0.3 m. The considered water levels can largely cover the lowest and largest water levels for the 50 yr extreme (ULS) in Table 1. Base case (LC0) environment (wind, wave, and current levels) with the heading of 0 deg is considered along with the water level changes.

Figures 23–25 compare the platform surge, heave, and pitch motions of maxima, minima, and mean (dot mark) due to water level variation. The maxima and minima values are from Equation (6). Here, water level 0 (zero) is the base case level. There are very small dynamic motion differences across the water levels. It is seen that mean heaves (setdowns) vary between positive and negative due to water level changes. The results suggest that the platform dynamic motions are likely affected very little by sea level changes.

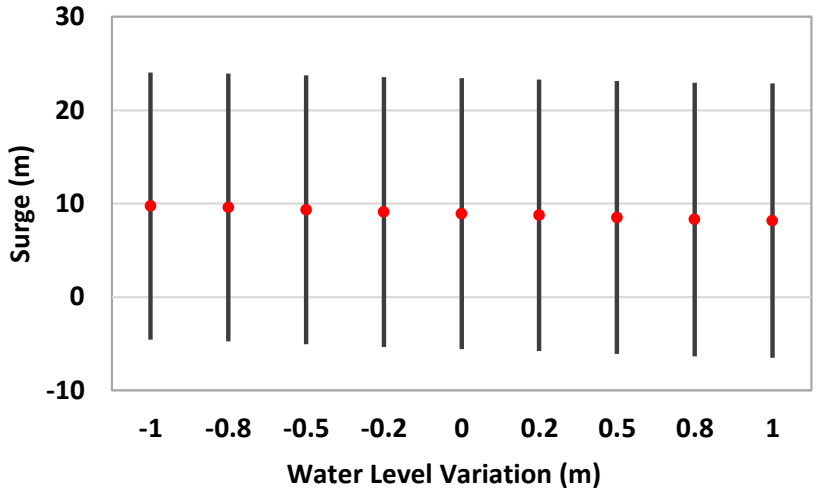


**Figure 23.** Platform surge motion for water level change (heading 0 deg).

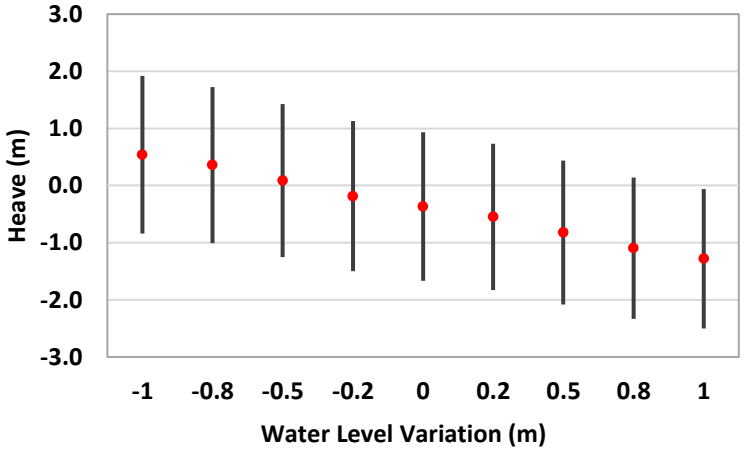


**Figure 24.** Platform heave motion for water level change (heading 0 deg).

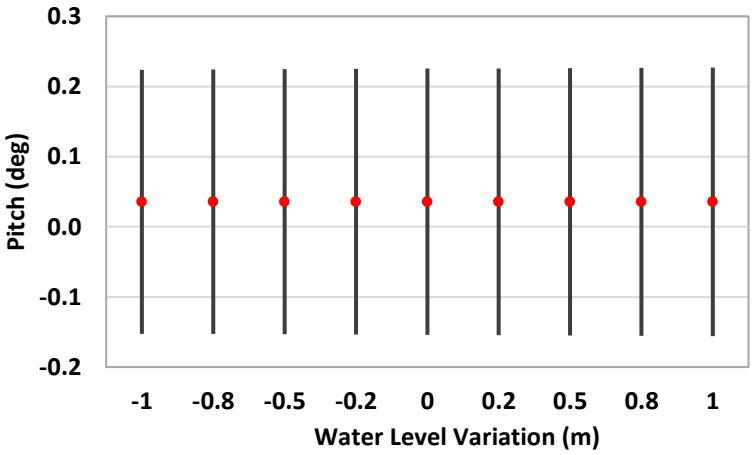


**Figure 25.** Platform pitch motion for water level change (heading 0 deg).

### 6.2.2. Maximum Tendon Tension

Figure 26 compares the maximum tension ratio to the T8 tension at water level 0 m ("T8_base case"). The results show that tensions increase almost linearly as the water level rises. Tension changes are in the range of about ±6% from the T8 tension at zero level. Utilization ratios in Figure 27 decrease with the increase in water level but they are greater than the required minimum of 1.0.

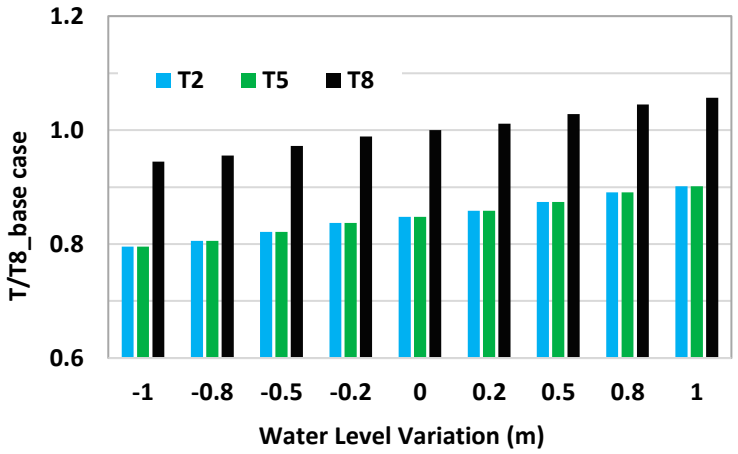


**Figure 26.** Maximum tension ratio to the base case T8 tension (heading 0 deg).

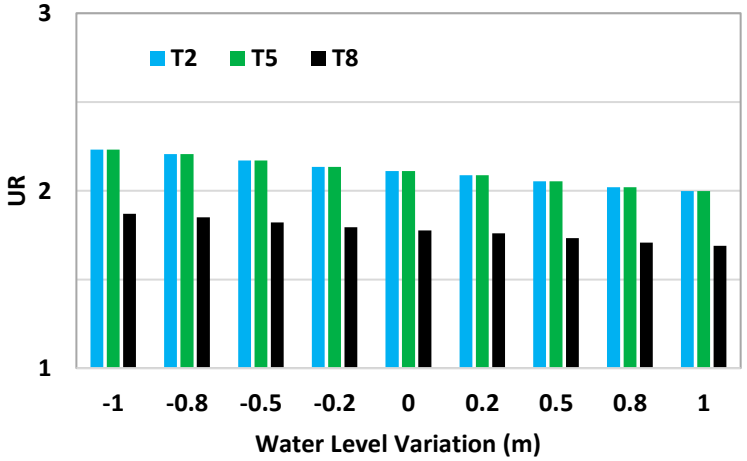


**Figure 27.** Tendon tension utilization ratio for water level change (heading 0 deg).

## 7. Conclusions

The concept design of a TLP-type floating platform to support a 15 MW turbine (KRISO-TLP) was completed to determine its feasibility for installation at a site located in the east offshore of South Korea. The platform was vertically moored with highly pretensioned nine-wire rope tendons. The platform and tendons are designed to withstand 50 years of extreme conditions. Additionally, the platform with the integrated turbine is designed to be wet-towable from the quayside without dedicated vessels to minimize the pre-service cost and risk.

An extreme response analysis under 50 yr extreme (parked) conditions was conducted to evaluate the platform motion, acceleration, airgap, and tendon tension considering wave height and period variation, intact and damaged tendons, environment heading change, and water level variation. The extreme responses analysis is as follows:

- The maximum platform offset ratio to the water depth for the intact and damaged tendon cases is below 20%. The offset ratio may be within an acceptable range, which is a future subject of research.
- The extreme responses are higher for the LCs with higher waves and for the LCs with shorter waves in the same wave height group.
- Horizontal accelerations at the nacelle height are much greater than vertical accelerations.
- Tendon damage causes a significant tendon tension increase in the remaining tendons in the damaged tendon group, while the lowest tension is observed in the intact tendon group.
- Tendon damage results in reduction of the mooring system stiffness, which can cause a swift of the platform heave and pitch frequencies to lower frequencies than those of the intact condition.
- The maximum DAF of the tendon tension is about 1.86 for the intact tendon and 3.0 for the damaged tendons.
- Maximum tendon tensions vary with the environment headings, which is in the range from −8% to +2% from the tension at 0 deg.
- Water level change can cause tension variations due to the change in platform buoyancy, while there are very small variations in platform dynamic motions.

It is confirmed that all design factors of the 15 MW TLP wind platform comply with the design criteria, including platform pitch, airgap, nacelle acceleration, and tendon strength (maximum and minimum tensions). This can conclude that the proposed TLP design with 15 MW can be applicable for the east offshore of South Korea, which is exposed to typhoon environments. Further design validation may include the study of high-frequency tendon tension, tendon fatigue, and flexible tower effects.

**Author Contributions:** Conceptualization, S.Y.B. and K.-H.K.; methodology, S.Y.B.; software, S.A.S.; formal analysis, S.Y.B. and S.A.S.; investigation, Y.-J.H. and K.-H.K.; data curation, J.-Y.P. and C.-H.L.; writing—original draft preparation, S.Y.B.; writing—review and editing, S.A.S., Y.-J.H. and S.A.S.; visualization, S.Y.B., J.-Y.P. and C.-H.L.; supervision, K.-H.K.; project administration, K.-H.K. and Y.-J.H.; funding acquisition, K.-H.K. All authors have read and agreed to the published version of the manuscript.

**Funding:** This work was supported by the "Development of Design Technology for TLP-type Floating Offshore Wind Turbine System and Scaled Model Test Technique" of the New and Renewable Energy of the Korea Institute of Energy Technology Evaluation and Planning (KETEP) grant funded by the Ministry of Trade, Industry, and Energy (MOTIE) (Nos. 20223030020130 and PNS5020).

**Institutional Review Board Statement:** Not applicable.

**Informed Consent Statement:** Not applicable.

**Data Availability Statement:** Data are contained within the article.

**Conflicts of Interest:** Authors Sung Youn Boo and Steffen Allan Shelley was employed by the company VL Offshore LLC. The remaining authors declare that the research was conducted in the absence of any commercial or financial relationships that could be construed as a potential conflict of interest.

## Abbreviations

The following abbreviations are used in this manuscript.

| | |
|---|---|
| ALS | Accidental Limit State |
| API | American Petroleum Institute |
| CoG | Center of Gravity |
| DAF | Dynamic Amplification Factor |
| DLC | Design Load Case |
| DNV | Det Norske Veritas |
| GM | Metacentric Height |
| IEA | International Energy Agency |
| LC | Load Case |
| JONSWAP | Joint North Sea Wave Observation Project |
| GW, MW | Gigawatt, Megawatt |
| MBL | Minimum Breaking Load |
| MSL | Mean Sea Line |
| NREL | National Renewable Energy Laboratory |
| NPD | Norwegian Petroleum Directorate |
| PSD | Power Spectral Density |
| RAO | Response Amplitude Operator |
| TLP | Tension Leg Platform |
| ULS | Ultimate Limit State |
| UR | Utilization Ratio |

## References

1. Ahn, H.-J.; Ha, Y.-J.; Park, S.-W.; Kim, K.-W. A Comparative study on the Response Characteristics of the Semi-submersible Platform of a 15 MW Floating Offshore Wind Turbine System in Operational Conditions. *J. Wind Energy* **2022**, *13*, 4.
2. Allen, C.; Viscelli, A.; Dagher, H.; Goupee, A.; Gaertner, E.; Abbas, N.; Hall, M.; Barter, G. *Definition of the UMaine VolturnUS-S Reference Platform Developed for the IEA Wind 15-Megawatt Offshore Reference Wind Turbine*; Technical Report; IEA Wind TCP Task 37; U.S. Department of Energy: Washington, DC, USA, 2020.
3. Wand, H.F.; Fan, Y.H.; Liu, Y. Dynamic Analysis of a Tension Leg Platform for Offshore Wind Turbines. *J. Power Technol.* **2014**, *94*, 42–49.
4. Available online: https://www.energyportzeeland.nl/data/formulieren/uploads/171128%20introduction%20blue%20h%20engineering.pdf (accessed on 24 January 2024).
5. Available online: http://www.oceanresource.co.uk/Ocean-Breeze.html (accessed on 24 January 2024).
6. Gueydon, S.; Wuillaume, P.; Jonkman, J.; Robertson, A.; Platt, A. Comparison of Second-Order Loads on a Tension-Leg Platform for Wind Turbines. In Proceedings of the Twenty-Fifth International Offshore and Polar Engineering Conference, Kona, HI, USA, 21–26 June 2015.

7. PelaStar TLP. 2024. Available online: https://pelastar.com/the-pelastar-tlp// (accessed on 5 January 2024).
8. Eco TLP. 2024. Available online: https://ecotlp.com/ (accessed on 5 January 2024).
9. Available online: https://www.sbmoffshore.com/newsroom/news-events/sbm-offshore-launches-float4windtm (accessed on 24 January 2024).
10. Yang, Y.; Bashir, M.; Wang, J.; Michailides, C.; Loughney, S.; Armin, M.; Hernandez, S.; Urbano, J.; Li, C. Wind-Wave Coupling Effects on the Fatigue Damage of Tendons for a 10 MW Multi-Body Floating Wind Turbine. *Ocean Eng.* **2020**, *217*, 107909. [CrossRef]
11. Suzuki, K.; Yamaguchi, H.; Akase, M.; Imakita, A.; Ishihara, T.; Fukumoto, Y.; Oyama, T. Initial design of tension leg platform for offshore wind farm. *J. Fluid Sci. Technol.* **2011**, *6*, 372–381. [CrossRef]
12. MODEC TLP. 2024. Available online: https://www.modec.com/business/newbiz/offshorewind.html (accessed on 5 January 2024).
13. Boo, S.Y.; Shelley, A.S.; Kim, D. A TLP Floating Foundation Design with Novel Tendon Mooring Technology for Hawaii Offshore Wind. In Proceedings of the Twenty-Ninth International Ocean and Polar Engineering Conference, Honolulu, HI, USA, 16–21 June 2019.
14. Adam, F.; Myland, T.; Dahlhaus, F.; Großmann, J. GICON-TLP for wind turbines—The path of development. In Proceedings of the 1st International Conference on Renewable Energies Offshore (RENEW), Lisbon, Portugal, 24–26 November 2014.
15. Pierella, F.; Avila, O.S.; Sanz, C.G.; Ashraf, A.; Aitor, N.A.; Kim, T. Numerical simulations of a 15MW wind turbine on a concrete TLP with rigid pipe tendons. *J. Phys. Conf. Ser.* **2022**, *2362*, 012030. [CrossRef]
16. Tetra TLP. 2023. Available online: https://www.stiesdal.com/offshore/tetra-offshore-foundations-for-any-water-depth (accessed on 5 January 2024).
17. Boo, S.Y.; Shelley, S.A.; Griffith, D.T.; Escalera Mendoza, A.S. Responses of a Modular Floating Wind TLP of MarsVAWT Supporting a 10 MW Vertical Axis Wind Turbine. *Wind* **2023**, *3*, 513–544. [CrossRef]
18. Shelley, S.A. Cost Analysis of 15MW Platforms for Horizontal and Vertical Axis Turbines for the West Coast U.S. Floating Wind Solution (FWS22), Houston. 2022. Available online: https://floatingwindsolutions.com/wp-content/uploads/2022/03/STEFFENSHELLEY_FWS-22-VLO-Presentation-2022-Feb-28.pdf (accessed on 24 January 2024).
19. Hsu, W.-T.; Litton, R.; Vasala, H.; Anderson, D.; Sheppard, R. Beneficial Wave Motion Response for Wind Turbine Support TLPs with Synthetic Rope Tendons. In Proceedings of the Offshore Technology Conference, Houston, TX, USA, 6–9 May 2019.
20. *DNV-ST-0119*; Det Norske Veritas (DNV). Floating Wind Turbine Structures. DNV: Oslo, Norway, 2021.
21. *API RP 2T*; Planning, Designing, and Constructing Tension Leg Platforms. American Petroleum Institute: Washington, DC, USA, 2010.
22. KRI-TLP-2023-EN-RPT-001, 2023, Basis of Design: 15 MW Class Floating Offshore Wind Turbine of TLP Type Development Project (Internal Document).
23. *DNV-RP-C205*; Environmental Conditions and Environmental Loads. DNV: Oslo, Norway, 2019.
24. Bae, Y.H.; Kim, M.H. Turbine-floater-tether coupled dynamic analysis including second-order sum-frequency wave loads for a TLP-type FOWT (floating offshore wind turbine). In Proceedings of the 32nd International Conference on Ocean, Offshore and Arctic Engineering, Nantes, France, 9–14 June 2013.
25. OrcaFlex—Dynamic Analysis Software for Offshore Marine Systems. Available online: https://www.orcina.com/orcaflex/ (accessed on 5 January 2024).
26. *DNV-ST-0437*; Loads and Site Conditions for Wind Turbines. DNV: Oslo, Norway, 2021.
27. Winterstein, S.; Ude, T.C.; Cornell., C.A.; Bjerager, P.; Haver, S. Environmental Parameters for Extreme Response: Inverse FORM with omission Sensitivity. In Proceedings of the ICOSSAR-93, Innsbruck, Austria, 9–13 August 1993.